RSC Advances

ROYAL SOCIETY OF CHEMISTRY

www.rsc.org/advances

Graphical Abstract

Small wear debris was constantly formed for the reiterative crush with the increase of sliding time t, resulting in the forming of anti-friction film, the lowering of wear rate of TiAl-10wt.%Ag and the stabilizing of prediction accuracy (from 97.60% to 97.62%) of prediction formula $W_4(t)$.
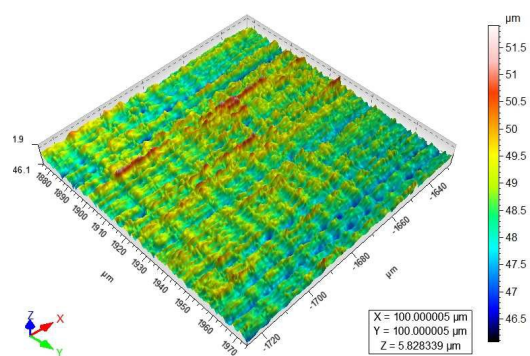
Wear rate of TiAl matrix composite containing 10wt.%Ag

predicted by Newton interpolation method

Kang Yang, Xiaoliang Shi*, Wenzheng Zhai, Ahmed Mohamed Mahmoud Ibrahim

School of Mechanical and Electronic Engineering, Wuhan University of Technology,

122 Luoshi Road, Wuhan 430070

Abstract: Using longevity of mechanical component was evaluated by predicting wear rate of material. The primary purpose of this study was to construct three prediction formulas ($W_4(F)$, $W_4(n)$ and $W_4(t)$) to predict wear rate at the different applied load F, rotate speed n and sliding time t based on TiAl matrix composite containing 10wt.%Ag. Prediction formulas of wear rate, which were constructed by the Newton interpolation method, were evaluated by making a comparison between testing error and computational error. The results showed that the prediction formulas ($W_4(F)$, $W_4(n)$ and $W_4(t)$) of wear rate were accepted for smaller computational error. It was found that the prediction accuracy gradually increased for the higher binding force of wear debris at larger applied load F (see formula $W_4(F)$), and slightly decreased for random impacting of wear debrises at the higher rotate speed n (see formula $W_4(n)$), as well as relatively stabilized for incessant forming of anti-friction film at different sliding time t (see formula $W_4(t)$).

Keywords: Metal matrix composites, microstructure, wear resistance, friction coefficient, wear mechanism

1. Introduction

In recent years, TiAl alloys have been paid extensive attention to satisfy the urgent

---

requirement of developed aerospace and automotive industries for the excellent mechanical behaviors and thermal behaviors[1-4]. However, TiAl alloys, for the poor tribological behaviors, was limited to further apply in the industrial field[5].

Tribological behaviors of TiAl alloys were significantly improved by fabricating TiAl matrix self-lubricating composite containing solid lubricants. Shi et al.[6] studied the tribological behavior of TiAl matrix composite containing 10wt.%Ag (TiAl-10wt.%Ag), and found that the friction coefficient and wear rate of TiAl-10wt.%Ag were lower than TiAl alloys at the temperatures of 25-400°C. Currently, many mechanical components of failure were caused for the excessive wear of materials. Hence, the wear-resistant of materials and the using longevity of mechanical components could be evaluated by investigating wear rate.

Many tribological researchers made the great effort to obtain the formula of wear rate. Archard[7] thought that weight loss only happened in the contact regions of matched surfaces during the sliding wear, and gave the definition of wear volume G, as shown in **formula 1**:

$$G = K \cdot L \cdot (\sigma_n / H) \tag{1}$$

where wear volume G was proportional to wear coefficient K, sliding distance L and normal stress σ_n, as well as inverse ratio to the hardness H of softer material. Kishore et al.[8] reported that in the initial stage, wear rate was mainly determined by applied load, and in the steady stage, wear rate mainly depended on the synergetic effect of applied load and sliding velocity. Boneh et al.[9] found that in the steady stage, wear rate was in linear relation with the applied load at a low velocity. Kasolang et al.[10]

detected that wear rate W_s was inverse ratio to sliding distance L, material density ρ and applied load F, and proportional to weight loss Δm. Wear rate W_s could be defined as **formula 2**:

$$W_s = \frac{\Delta m}{L \cdot \rho \cdot F} \tag{2}$$

Gong et al.[11] thought that during the dry sliding, wear debris was continually oxidized, resulting in generating of massive oxides, lowering weight loss Δm. Consequently, wear volume V could be adopted to better calculate wear rate for containing the generated oxides. Wear rate formula W_s was optimized as **formula 3**:

$$W_s = \frac{V}{F \cdot L} \tag{3}$$

Currently, wear rate **formula 3** was widely accepted by tribological researchers. However, wear volume V needed to be measured after each tribological test, leading to the poor prediction of **formula 3** of wear rate, and the waste of energy and material. The test conditions of applied load F, rotate speed n and sliding time t were needed to be chosen before tribological tests based on the ball-on-disk tribometer. Hence, the **formula 3** of wear rate would be further optimized as the formula of applied load F, rotate speed n, sliding time t and cross-section area A of wear scar, in order to construct the prediction formula of wear rate. The method of Newton interpolation was not restrained by the increasing interpolation nodes, and the measured values (wear rate W_s) at the different interpolation nodes $((W_s, F), (W_s, n)$ and (W_s, t)) were not influenced by the formula structured using the method of Newton interpolation. Cui et al.[12] adopted the method of Newton interpolation to predict the state of charge, and found that the method of Newton interpolation could be well adopted to predict

the charge state of lead batteries. Hence, the Newton interpolation method was chosen to construct the prediction formula of wear rate. To our best knowledge, few works currently reported the prediction formula of wear rate in the form of Newton interpolation polynomial.

In this study, TiAl-10wt.%Ag, for its excellent tribological behavior, was chosen as test material. The prediction formula of wear rate was constructed by the Newton interpolation method after three steps. **Step 1:** F**ormula 3** was optimized as the wear rate formula W_s of applied load F, rotate speed n, sliding time t and cross-section area A of wear scar. **Step 2:** Three cross-section area formulas $A_4(F)$, $A_4(n)$ and $A_4(t)$ ($A_4(F)$ between A and F, $A_4(n)$ between A and n, as well as $A_4(t)$ between A and t) were constructed using the Newton interpolation method based on five equidistant interpolation nodes, respectively. **Step 3:** Three prediction formulas ($W_4(F)$, $W_4(n)$ and $W_4(t)$) in the form of Newton interpolation polynomial were respectively obtained by substituting the formulas $A_4(F)$, $A_4(n)$ or $A_4(t)$ into the optimized formula W_s of wear rate. Three prediction formulas ($W_4(F)$, $W_4(n)$ and $W_4(t)$) of wear rate were respectively evaluated by making a comparison between computational error and testing error. Different computational error was reasonably interpreted by wear mechanisms at the different applied load F, rotate speed n or sliding time t. The prediction formulas ($W_4(F)$, $W_4(n)$ and $W_4(t)$) of wear rate could be adopted to evaluate the using longevity of the important machinery components by predicting wear rate at the different applied load F, rotate speed n or sliding time t.

2. Experimental details

2.1 Materials

TiAl-10wt.%Ag (48at.%Ti-47at.%Al-2at.%Cr-2at.%Nb-1at.%B-10wt.%Ag), which was fabricated by spark plasma sintering (SPS), was composed of Ti, Al, B, Nb, Cr and Ag. Before being fabricated, the powders of Ti, Al, B, Nb, Cr and Ag were loaded into in the teflon vials, and then mixed by a vibration milling (45Hz in frequency). After being mixed and dried, the powders were sealed in the cylindrical graphite mold (25mm in inner diameter), and sintered using a D.R. Sinter$^®$ SPS3.20 apparatus (made in Sumitomo Coal & Mining, now SPS Syntex Inc.) for 8min at the temperature and pressure of 1000$°C$ and 30MPa in pure Ar atmosphere protection. The heating rate of 100$°C/min$ was chosen.

2.2 Vicker's microhardness and density

Vicker's hardness of TiAl-10wt.%Ag was measured by the Vicker's hardness apparatus according to ASTM standard E92-82[13]. To attain the mean hardness of 5.97GPa, ten tests were repeatedly carried out at a load of 10N. The mean density of 4.22g/cm^3 was acquired using Archimedes' principle in terms of ASTM Standard B962-08[14].

2.3 Tribological test

To investigate the tribological property of TiAl-10wt.%Ag, tribological tests were carried out on the ball-on-disk high temperature tribometer of HT-1000 (made in Zhong Ke Kai Hua Corporation, China) according to ASTM Standard G99-95[15]. The cylindrical sample of the diameter and height of 25mm and 8mm acted as the rotary disk against the stationary Si_3N_4 ball of 6mm diameter. The districts *[1.65N, 11.65N]*,

[56r/min, 504r/min] and *[900s, 4500s]* were respectively chosen for the applied load

F(N (Newton)*)*, rotate speed *n(r/min* (revolutions per minute)*)* and sliding time *t(s*

(second)*)*. At 45-65% relative humidity, three tests were repeatedly carried out to

obtain mean wear rate under the different conditions of tribological test, as shown in

Table 1.

Table 1 Tribological test at different applied load *F*, rotate speed *n* or sliding time *t*

Test conditions	*F*-392-3600 (*N-r/min-s*)	9.15-*n*-3600 (*N-r/min-s*)	9.15-392-*t* (*N-r/min-s*)
1	*1.65*-392-3600	9.15-*56*-3600	9.15-392-*900*
2	*4.15*-392-3600	9.15-*168*-3600	9.15-392-*1800*
3	*6.65*-392-3600	9.15-*280*-3600	9.15-392-*2700*
4	*9.15*-392-3600	9.15-*392*-3600	9.15-392-*3600*
5	*11.65*-392-3600	9.15-*504*-3600	9.15-392-*4500*

2.4 Microstructure analysis

TiAl-10wt.%Ag was examined by XRD with Cu Karadiation at 30kV and 40mA at

a scanning speed of $0.01^{o}s^{-1}$. Cross-section area *A* of wear scar was measured by the

surface profiler of ST400 (Nanovea). Wear scar morphology was analyzed by the

electron probe microanalysis of JAX-8230 (EPMA).

3. Results and discussion

3.1 Compositions of TiAl-10wt.%Ag

Fig.1 showed the typical XRD pattern of TiAl-10wt.%Ag fabricated by SPS. As

was clear in this pattern, it can be concluded from the different diffraction peaks that

TiAl-10wt.%Ag was mainly composed of TiAl, TiC and Ag.

6
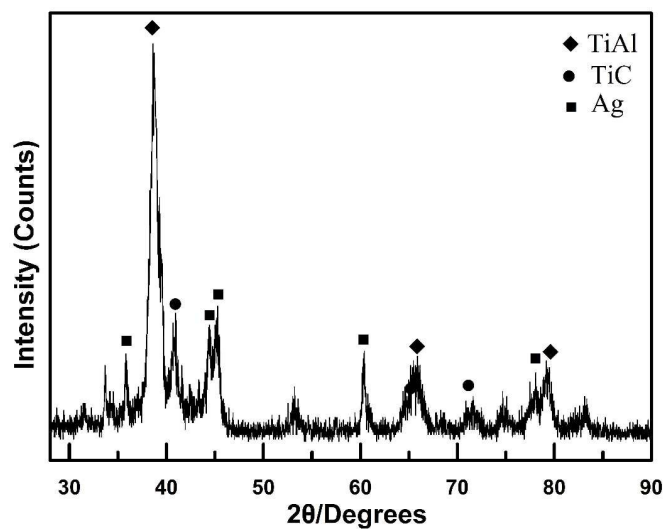
Fig.1 Typical XRD pattern of TiAl-10wt.%Ag fabricated by SPS
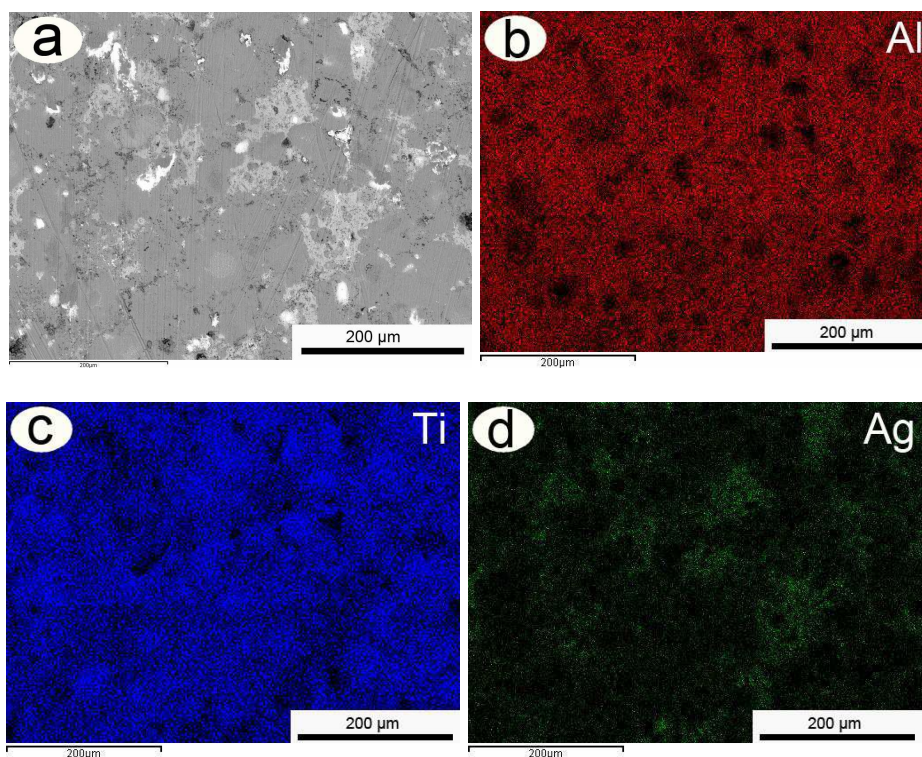
Fig.2 Microstructure and elemental distribution of TiAl-10wt.%Ag

Fig.**2** exhibited the microstructure and elemental distribution of TiAl-10wt.%Ag. It was clearly seen in **Fig**.**2** that the solid lubricant Ag was uniformly distributed in TiAl matrix composite.

7

3.2 Optimizing formula of wear rate

To construct three cross-section area formulas $A_4(F)$, $A_4(n)$ and $A_4(t)$ in the form of Newton interpolation polynomial, **formula 3** needed to be further optimized.

Wear volume V in **formula 3** can be written as **formula 4**[16]:

$$V = A \cdot C \tag{4}$$

Wear volume V was additionally rewritten as **formula 5** for $C=2 \cdot \pi \cdot R$:

$$V = 2 \cdot A \cdot \pi \cdot R \tag{5}$$

where A was cross-section area of wear scar in mm^2, C was perimeter of wear scar in mm, R was mean radius of wear scar in mm. Cross-section area A of wear scar could be measured by the surface profiler of ST400. **Fig.3** showed the profile of wear scar of TiAl-10wt.%Ag. When the measured stylus of surface profiler slowly moved across wear scar along the straight line BB (see **Fig.3b**), the cross-section area A of wear scar (see **Fig.3a**) gradually formed by recording the coordinate positions of measured stylus.

Sliding distance L in **formula 3** was also expressed as **formula 6** for $v=(\pi \cdot R \cdot n)/30$:

$$L = v \cdot t = \frac{1}{30} \cdot \pi \cdot R \cdot n \cdot t \tag{6}$$

where v, n, t were sliding velocity in m/s, rotate speed in r/min and sliding time in r/min, respectively.

8
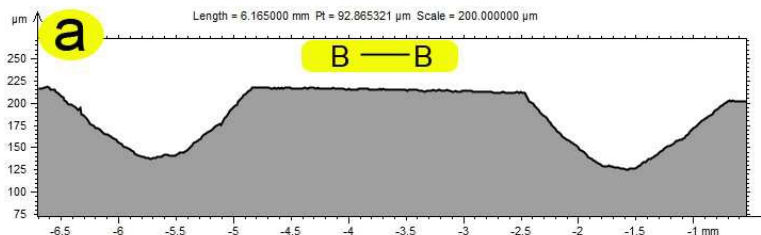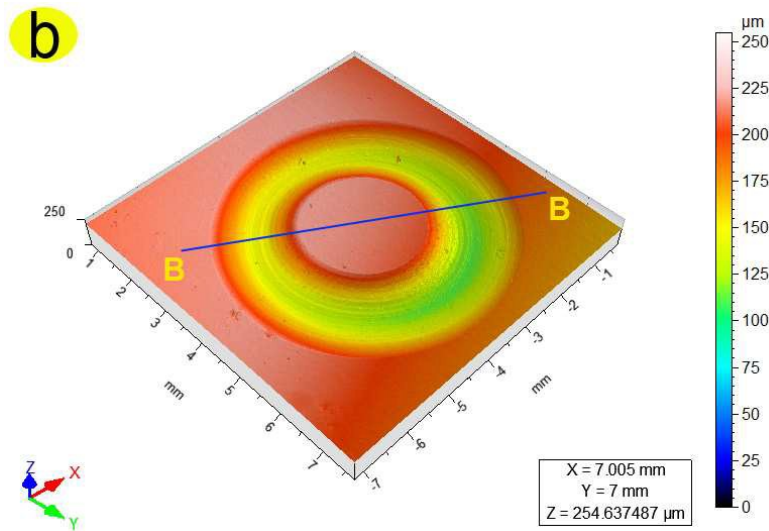
Fig.3 Profile of wear scar of TiAl-10wt.%Ag: two-dimension profile of wear scar (a)

and three-dimension profile of wear scar (b)

Based on the ball-on-disk tribometer, **formula 3** could be optimized as **formula 8**

by substituting **formula 5** and **formula 7** into **formula 3**:

$$W_s = 60 \cdot \frac{A}{F \cdot n \cdot t} \tag{7}$$

where W_s was wear rate in $mm^2/(N \cdot r/min \cdot s)$. The units of cross-section area A, applied

load F, rotate speed n and sliding time t were mm^2, N, r/min and s, respectively.

Hence, the unit of wear rate W_s could be expressed as $mm^2/(N \cdot r/min \cdot s)$.

3.3 Wear rate

Fig.4 showed the mean wear rate at the different applied load F, rotate speed n and

sliding time t. As shown in **Fig.4**a, wear rate continually decreased with the increasing

of applied load F. As was clear in **Fig.4**b, wear rate exhibited the fluctuantly upward

tendency with the increase of rotate speed n. It can be seen from **Fig.4**c that wear rate

showed the continually downward tendency with the increasing of sliding time t.

9
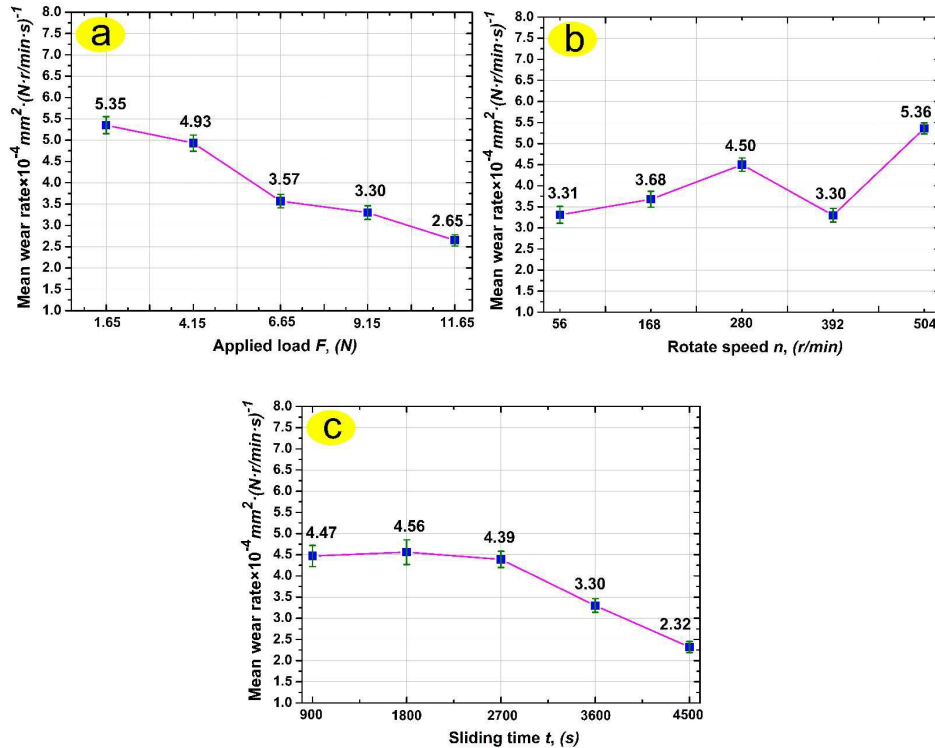
Fig.4 Mean wear rate at the different applied load *F* (a), rotate speed *n* (b) and sliding time *t* (c)

In order to evaluating using longevity of mechanical component at the different applied load *F*, rotate speed *n* and sliding time *t*, wear rate could be predicted by constructing three prediction formulas of wear rate. Three cross-section area formulas $A_4(F)$, $A_4(n)$ and $A_4(t)$ needed to be firstly constructed using the method of Newton interpolation.

3.4 Definition

The method of Newton interpolation was adopted to construct cross-section area formulas $A_4(F)$, $A_4(n)$ and $A_4(t)$. The prediction fourmulas $W_4(F)$, $W_4(n)$ and $W_4(t)$ of wear rate were respectively obtained by substituting formulas $A_4(F)$, $A_4(n)$ and $A_4(t)$ into **Formula 7**. Before be applying, prediction fourmulas $W_4(F)$, $W_4(n)$ and $W_4(t)$ in the form of Newton interpolation polynomial needed to be respectively evaluated by

10

making a comparison between testing error and computational error. Hence, the definitions of Newton interpolation, testing error, computational error and prediction accuracy were required to given in the following sections.

3.4.1 Definition of Newton interpolation[17]

It was supposed that a function $y=f(x)$ was known at the $M+1$ points of $(x_0, y_0), \cdots, (x_m, y_m)$, where the values x_k were spread out in the district $[a, b]$ and satisfied $y_k = f(x_k)$ for $k=0, 1, \cdots, m$, namely:

$$a \leq x_0 < x_1 < \cdots < x_M \leq b \quad \text{and} \quad y_k = f(x_k) \tag{8}$$

When $p_k(x_k)$ was equivalent to $y=f(x_k)$ at $x=x_k$. Based on these $M+1$ points, the polynomial $p_M(x)$ of m degree was constructed in order to approximate $y=f(x)$ in the district $[a, b]$. Hence, the polynomial $p_M(x)$ was called the interpolation polynomial. $[a, b]$ was interpolation district. $(x_0, y_0), \cdots, (x_m, y_m)$ were known as interpolation nodes. The method, which was adopted to approximate function $y=f(x)$, was called as the method of Newton interpolation.

It was assumed that $p_M(x)$ was the interpolation polynomial of m degree, which could be defined as **formula 9**:

$$p_M(x) = a_0 + a_1 x + \cdots + a_k x^m \tag{9}$$

where $a_0, a_1, \cdots, a_k$ were the coefficients of Newton interpolation polynomial for $k=0, 1, \cdots, m$. These $M+1$ interpolation nodes of $(x_0, y_0), \cdots, (x_m, y_m)$ could be used to construct the interpolation polynomial $p_M(x)$ of at most m degree. F**ormula 9** could be redefined as **formula 10** to satisfy **formula 11:**

$$p_M(x) = a_0 + a_1 \cdot (x - x_0) + \cdots + a_m \cdot (x - x_0) \cdot (x - x_1) \cdots (x - x_{m-1}) \tag{10}$$

11

$$f(x_j) = p_N(x_j) \qquad \text{for} \quad j = 0, 1, \cdots, m \tag{11}$$

where $1,\ x-x_0, \cdots, (x-x_0)\cdots(x-x_{m-1})$ were known as primary function. Coefficient a_0 was

the solution of function $y=f(x)$ at $x=x_0$, namely: $y_0=f(x_0)$ at $x=x_0$. Coefficients $a_1,$

$a_2,\cdots,a_m$ can be expressed by forward differences $\Delta f_0/h,\ \Delta^2 f_0/(2 \cdot h), \cdots, \Delta^m f_0/(m! \cdot h^m)$. h

was the step size of equidistant interpolation nodes of $x_0,\ x_1, \cdots, x_m$, namely: $h=x_{k+1}-x_k$.

The forward differences $\Delta f_k,\ \Delta^2 f_k, \cdots, \Delta^m f_k$, which were known as the forward difference

of first, second, $\cdots$, m order, could be defined as **formula 15**:

$$\Delta f_k = f_{k+1}(x_{k+1}) - f_k(x_k)$$

$$\Delta^2 f_k = \Delta f_{k+1}(x_{k+1}) - \Delta f_k(x_k)$$

$$\vdots \tag{12}$$

$$\Delta^m f_k = \Delta^{m-1} f_{k+1}(x_{k+1}) - \Delta^{m-1} f_k(x_k)$$

When variable x was supposed as $x_0+e \cdot h$, namely: $x= x_0+e \cdot h$. e could be written as

$(x-x_0)/h=(x-x_0)/(x_{k+1}-x_k)$ for $h=x_{k+1}-x_k$, namely: $e=(x-x_0)/h=(x-x_0)/(x_{k+1}-x_k)$. Hence,

Formula 10 was written as **formula 13** by substituting **Formula 12** into **Formula 10**:

$$p_M(x) = f_0(x_0) + e \cdot \Delta f_0 + \frac{1}{2!} \cdot e \cdot (e-1) \cdot \Delta^2 f_0 + \cdots + \frac{e \cdot (e-1) \cdots (e-m+1)}{m!} \cdot \Delta^m f_0 \tag{13}$$

In this study, five interpolation nodes were chosen, **Formula 13** was additionally

rewritten as **formula 14** for $e=(x-x_0)/h=(x-x_0)/(x_{k+1}-x_k)$:

$$p_4(x) = f_0(x_0) + \frac{x-x_0}{h} \cdot \Delta f_0 + \frac{1}{2!} \cdot \frac{x-x_0}{h} \cdot \left(\frac{x-x_0}{h} - 1\right) \cdot \Delta^2 f_0 + \frac{1}{3!} \cdot \frac{x-x_0}{h} \cdot \left(\frac{x-x_0}{h} - 1\right) \cdot$$

$$\left(\frac{x-x_0}{h} - 2\right) \cdot \Delta^3 f_0 + \frac{1}{4!} \cdot \frac{x-x_0}{h} \cdot \left(\frac{x-x_0}{h} - 1\right) \cdot \left(\frac{x-x_0}{h} - 2\right) \cdot \left(\frac{x-x_0}{h} - 3\right) \cdot \Delta^4 f_0 \tag{14}$$

where $\Delta f_0,\ \Delta^2 f_0,\ \Delta^3 f_0$ and $\Delta^4 f_0$, which were respectively known as the forward

differences of first, second, third and fourth order, could be obtained in **Table 2**. In

order to simplify the application of Newton interpolation method, based on the

software of MATLAB7, the small programming was developed to construct the prediction formulas ($W_4(F)$, $W_4(n)$ and $W_4(t)$) of wear rates.

Table 2 Forward differences for constructing Newton interpolation polynomial $p_4(x)$

x_k	$f_k(x_k)$	Δf	$\Delta^2 f$	$\Delta^3 f$	$\Delta^4 f$
x_0	$f_0(x_0)$	$\Delta f_0 = f_1(x_1) - f_0(x_0)$	$\Delta^2 f_0 = \Delta f_1 - \Delta f_0$	$\Delta^3 f_0 = \Delta^2 f_1 - \Delta^2 f_0$	$\Delta^4 f_0 = \Delta^3 f_1 - \Delta^3 f_0$
x_1	$f_1(x_1)$	$\Delta f_1 = f_2(x_2) - f_1(x_1)$	$\Delta^2 f_1 = \Delta f_2 - \Delta f_1$	$\Delta^3 f_1 = \Delta^2 f_2 - \Delta^2 f_1$	
x_2	$f_2(x_2)$	$\Delta f_2 = f_3(x_3) - f_2(x_2)$	$\Delta^2 f_2 = \Delta f_3 - \Delta f_2$		
x_3	$f_3(x_3)$	$\Delta f_3 = f_4(x_4) - f_3(x_3)$			
x_4	$f_4(x_4)$				

3.4.2 Definitions of testing error, computational error and prediction accuracy

In order to evaluate the prediction formulas $W_4(F)$, $W_4(n)$ and $W_4(t)$ of wear rate, the comparison between testing error and computational error needed to be conducted at the different applied load F, rotate speed n and sliding time t. The testing error E_{test} and computational error E_{comp} were respectively expressed as **formulas 15** and **16**:

$$E_{test} = \frac{\left| W_{test} - W_{mean-test} \right|}{W_{mean-test}} \cdot 100\% \tag{15}$$

where E_{test} was testing error, W_{test} was testing wear rate, $W_{mean-test}$ was the mean wear rate of three tests.

$$E_{\mathbf{comp}} = \frac{\left| W_{comp} - W_{mean-test} \right|}{W_{mean-test}} \cdot 100\% \tag{16}$$

where E_{comp} was computational error, W_{comp} was computational wear rate using the wear rate formulas $W_4(F)$, $W_4(n)$ or $W_4(t)$.

Prediction accuracy was improved with the decreasing of computational error.

Hence, the prediction accuracy of prediction formula of wear rate could be defined as

formula 17:

$$P(F,n)_{\mathbf{comp}} = 1 - E(F,n)_{\mathbf{comp}} = 1 - \frac{\left|W(F,n)_{comp} - W(F,n)_{mean-test}\right|}{W(F,n)_{mean-test}} \cdot 100\% \tag{17}$$

3.5 Applied load F

3.5.1 Constructing prediction formula $W_4(F)$ of wear rate

Cross-section area formula $A_4(F)$ **(**$A_4(F)$ between *A* and *F***)** needed to be constructed

using the method of Newton interpolation, in order to construct the prediction formula

$W_4(F)$ of wear rate.

Five equidistant interpolation nodes of *(F_0, A_0), (F_1, A_1), (F_2, A_2), (F_3, A_3)* and *(F_4,*

A_4) were chosen as *(1.65, 2.07×10⁻²), (4.15, 4.81×10⁻²), (6.65, 5.58×10⁻²), (9.15,*

7.11×10⁻²) and *(11.65, 7.27×10⁻²)*. **Table 3** showed the forward differences at the

different applied load *F*. Hence, in the applie load district *[1.65N, 11.65N]*,

cross-section area formula $A_4(F)$ was defined as **formula 18** by the method of Newton

interpolation:

$$\begin{aligned} A_4(F) = (2.07 + 2.74 \cdot \left(\frac{F}{2.5} - 0.66\right) - 0.985 \cdot \left(\frac{F}{2.5} - 0.66\right) \cdot \left(\frac{F}{2.5} - 1.66\right) + \\ 0.455 \cdot \left(\frac{F}{2.5} - 0.66\right) \cdot \left(\frac{F}{2.5} - 1.66\right) \cdot \left(\frac{F}{2.5} - 2.66\right) - \\ 0.2025 \cdot \left(\frac{F}{2.5} - 0.66\right) \cdot \left(\frac{F}{2.5} - 1.66\right) \cdot \left(\frac{F}{2.5} - 2.66\right) \cdot \left(\frac{F}{2.5} - 3.66\right)) \times 10^{-2} \end{aligned} \tag{18}$$

14

Table 3 Forward differences at the different applied load F

Applied load $F(N)$	$A(F)$	$\Delta A(F)$	$\Delta^2 A(F)$	$\Delta^3 A(F)$	$\Delta^4 A(F)$
1.65 (F_0)	2.07×10^{-2}	2.74×10^{-2}	-1.97×10^{-2}	2.73×10^{-2}	-4.86×10^{-2}
4.15 (F_1)	4.81×10^{-2}	0.77×10^{-2}	0.76×10^{-2}	-2.13×10^{-2}	
6.65 (F_2)	5.58×10^{-2}	1.53×10^{-2}	-1.37×10^{-2}		
9.15 (F_3)	7.11×10^{-2}	0.16×10^{-2}			
11.65 (F_4)	7.27×10^{-2}				

Fig.5 showed the curve graph of cross-section area formula $A_4(F)$ at the different applied load F. As was obvious in **Fig.5**, cross-section area A exhibited the upward tendency with the increasing of applied loads of 1.65-11.65N.
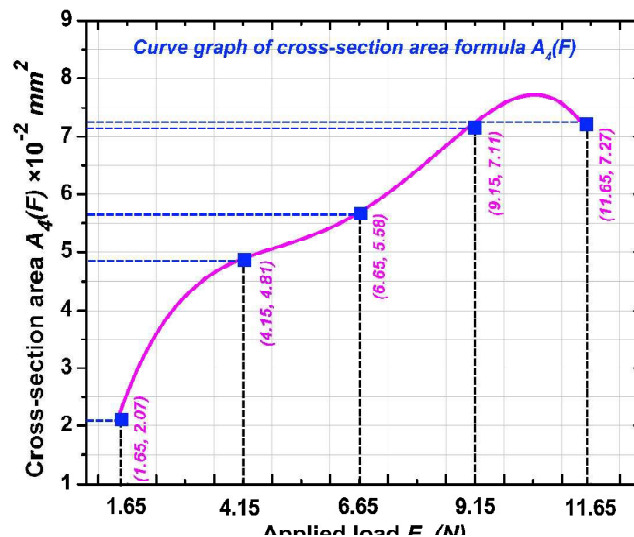
Fig.5 Curve graph of cross-section area formula $A_4(F)$ at the different applied load F

In the applied load district *[1.65N, 11.65N]*, prediction formula $W_4(F)$ of wear rate was defined as **formula 19** by substituting cross-section area **formula** $A_4(F)$ (see **formula 18**) into **formula 7:**

15

$$W_s(F) = \frac{60}{F \cdot n \cdot t} \cdot A_4(F) = \frac{1}{23520 \cdot F} \cdot 10^{-2} \cdot \left(2.07 + 2.74 \cdot \left(\frac{F}{2.5} - 0.66\right) - 0.985 \cdot \right.$$

$$\left(\frac{F}{2.5} - 0.66\right) \cdot \left(\frac{F}{2.5} - 1.66\right) + 0.455 \cdot \left(\frac{F}{2.5} - 0.66\right) \cdot \left(\frac{F}{2.5} - 1.66\right) \cdot \left(\frac{F}{2.5} - 2.66\right) \tag{19}$$

$$\left. -0.2025 \cdot \left(\frac{F}{2.5} - 0.66\right) \cdot \left(\frac{F}{2.5} - 1.66\right) \cdot \left(\frac{F}{2.5} - 2.66\right) \cdot \left(\frac{F}{2.5} - 3.66\right)\right)$$

Fig.6 Curve chart of prediction formula $W_4(F)$ of wear rate at the different

applied load F

    Fig.6 showed the curve chart of prediction formula $W_4(F)$ of wear rate at the different applied load F. It can be seen in **Fig.6** that wear rate continuously decreased with the increasing of applied load F. It may be concluded that the pressure stress was improved with the increase of applied load F. Bulk wear debris was crushed into many small wear debris at the higher pressure stress, resulting in improving of contact areas of wear debris, strengthening of binding forces of wear debris and lowering of material loss of TiAl-10wt.%Ag. Consequently, TiAl-10wt.%Ag exhibited the smaller wear rate.

3.5.2 Evaluating prediction formula $W_4(F)$ of wear rate

    Table 6 showed the comparative analysis between testing error and computational

error **2.90**-392-3600 and **10.40**-392-3600 (**N**-r/min-s). As shown in **Table 6**, wear rate

showed the downward tendency with the increase of applied load F. Simultaneously,

the computational error was smaller than testing error at the different applied load F.

Hence, in the district *[1.65N, 11.65N]*, the formula $W_4(F)$ was accepted to predict

wear rate for the small computational error.

Table 6 Comparative analysis between testing error and computational error at

2.90-392-3600 and **10.40**-392-3600 (*N*-r/min-s)

Test conditions	**2.90**-392-3600			**10.40**-392-3600		
W_{test}	6.20	5.86	5.47	3.43	3.09	2.89
E_{test}	6.10%	0.29%	6.34%	9.35%	1.49%	7.86%
W_{comp}		5.93			3.13	
E_{comp}		1.48%			0.32%	

3.5.3 Influence of wear mechanisms on prediction accuracy

Fig.7 exhibited the typical electron probe morphologies of wear scar after 80min

sliding at the different applied load F. As shown in **Fig.7**a, the primary wear

mechanism was abrasive wear at **2.90**-392-3600 (*N*-r/min-s) for bulk wear debris on

the smooth wear scar. As was clear in **Fig.7**b, the small wear debris and discontinuous

wear grooves appeared on wear scar. It was apparent that the main wear mechanisms

were abrasive wear and plough at **10.40**-392-3600. The pressure stress was

continually improved with the increase of applied load F, resulting in cracking of bulk

wear debris into small wear debris, improving of contact areas of wear debris,

strengthening of binding forces of wear debris, converting of wear mechanisms and

17

lowering of wear rate of TiAl-10wt.%Ag, as well as improving of prediction accuracy

of formula $W_4(F)$ (see **formula 19**). Hence, the wear rate of TiAl-10wt.%Ag was

smaller at the higher applied load F. Simultaneously, the small wear debris was

retained on wear scar by the deep wear groove at **10.40**-392-3600.
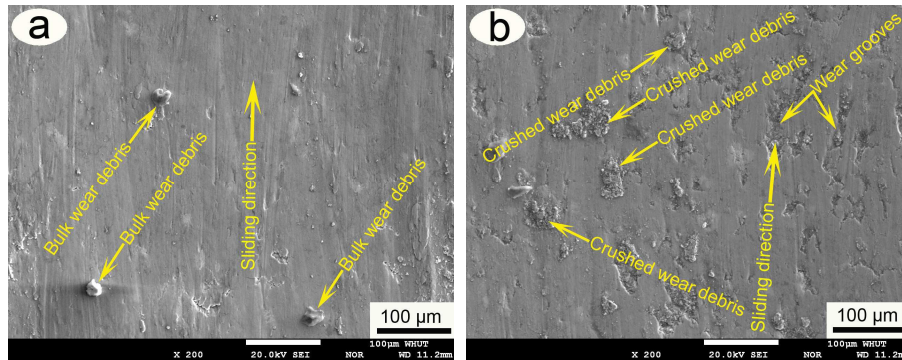
Fig.7 Typical electron probe morphologies of wear scar after 80min sliding at the

different applied load F: **2.90**-392-3600 (a), **10.40**-392-3600 (b)

3.5.4 Influence of surface textures on prediction accuracy

Excellent surface texture of wear scar, which was determined by the height

parameters of small Sa, Sq and Sku, was beneficial to the improving of contact area,

lowering of contact stress and acquiring of smoothe wear scar. Mean surface

roughness was measured by the arithmetical mean height (Sa). Standard deviation of

height distribution was evaluated by the root mean square height (Sq). Flatness of

height distribution could be examined by the kurtosis of height distribution (Sku).
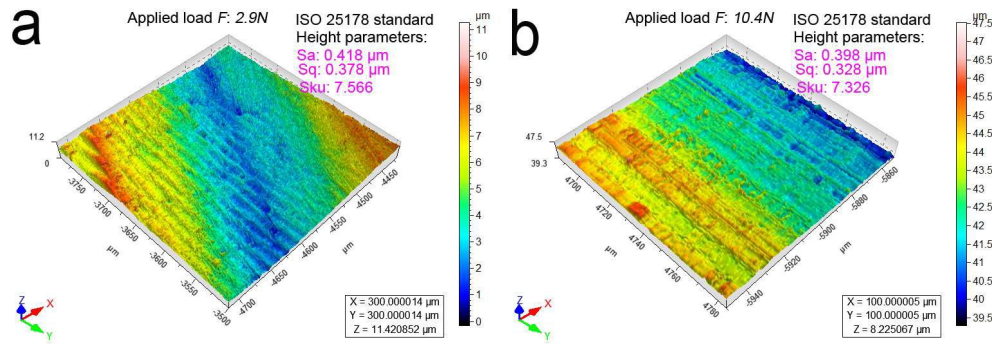
Fig.8 Representative surface texture of wear scar at the different applied load *F*:

2.90-392-3600 (a), **10.40**-392-3600 (b)

Fig.8 showed the representative surface texture of wear scar at the different applied

load *F*. The more smoother wear scar was obtained for the smaller Sa (0.398 μm), Sq

(0.328 μm) and Sku (7.326) at **10.40**-392-3600 (*N*-r/min-s), if compared to those at

2.90-392-3600. It can be concluded that wear debris was refined at the high applied

load of 10.40N, resulting in smoothing of wear scar and improving of prediction

accuracy (99.68%) of formula $W_4(F)$.

Due to wear rates were mainly determined by the applied load *F* and rotate speed *n*,

it was rather significant to study wear rate at the different rotate speed *n*.

3.6 Rotate speed n

3.6.1 Constructing prediction formula $W_4(n)$ of wear rate

Newton interpolation method could be used to construct cross-section area formula

$A_4(n)$ **(**$A_4(n)$ between *A* and *n***)** to obtain the prediction formula $W_4(n)$ of wear rate.

Five interpolation nodes were chosen as *(56, 1.02×10^{-2})*, *(168, 3.39×10^{-2})*, *(280,*

6.91×10^{-2}), *(392, 7.11×10^{-2})* and *(504, 14.83×10^{-2})*. **Table 4** showed the forward

differences at the different rotate speed *n*. Hence, in the rotate speed district *[56r/min,*

504r/min], cross-section area formula $A_4(n)$ was defined by the method of Newton

interpolation, as shown in **formula 20**:

$$A_4(n) = A_4(n_0 + e_n \cdot h_n) = \left(\mathbf{1.02} + \mathbf{2.37} \cdot \left(\frac{n}{112} - 0.5\right) + \mathbf{0.5741} \cdot \left(\frac{n}{112} - 0.5\right)\right.$$
$$\cdot \left(\frac{n}{112} - 1.5\right) - \mathbf{0.7447} \cdot \left(\frac{n}{112} - 0.5\right) \cdot \left(\frac{n}{112} - 1.5\right) \cdot \left(\frac{n}{112} - 2.5\right) + \tag{20}$$
$$\left.\mathbf{0.6379} \cdot \left(\frac{n}{112} - 0.5\right) \cdot \left(\frac{n}{112} - 1.5\right) \cdot \left(\frac{n}{112} - 2.5\right) \cdot \left(\frac{n}{112} - 3.5\right)\right) \times 10^{-2}$$

Table 4 Forward differences at the different rotate speed n

Rotate speed n	$A(n)$	$\Delta A(n)$	$\Delta^2 A(n)$	$\Delta^3 A(n)$	$\Delta^4 A(n)$
56 (n_0)	1.02×10^{-2}	2.37×10^{-2}	1.15×10^{-2}	-4.47×10^{-2}	15.31×10^{-2}
168 (n_1)	3.39×10^{-2}	3.52×10^{-2}	-3.32×10^{-2}	10.84×10^{-2}	
280 (n_2)	6.91×10^{-2}	0.20×10^{-2}	7.52×10^{-2}		
392 (n_3)	7.11×10^{-2}	7.72×10^{-2}			
504 (n_4)	14.83×10^{-2}				

Fig.9 exhibited the curve graph of formula $A_4(n)$ of cross-section area of wear scar at the different rotate speed n. As shown in **Fig.9**, cross-section area A continuously increased with the increasing of rotate speeds of 56-504r/min.

In the district *[56r/min, 504r/min]*, predicted formula $W_4(n)$ of wear rate was defined as **formula 21** by substituting cross-section area **formula** $A_4(n)$ (see **formula 20**) into **formula 7**:

$$W_s(n) = \frac{\mathbf{60}}{F \cdot n \cdot t} \cdot A_4(n) = \frac{\mathbf{1}}{\mathbf{549} \cdot n} \cdot 10^{-2} \cdot \left(\mathbf{1.0183} + \mathbf{2.3717} \cdot \left(\frac{n}{112} - 0.5\right) + \mathbf{0.5741} \cdot\right.$$
$$\left(\frac{n}{112} - 0.5\right) \cdot \left(\frac{n}{112} - 1.5\right) - \mathbf{0.7447} \cdot \left(\frac{n}{112} - 0.5\right) \cdot \left(\frac{n}{112} - 1.5\right) \cdot \left(\frac{n}{112} - 2.5\right) + \tag{21}$$
$$\left.\mathbf{0.6379} \cdot \left(\frac{n}{112} - 0.5\right) \cdot \left(\frac{n}{112} - 1.5\right) \cdot \left(\frac{n}{112} - 2.5\right) \cdot \left(\frac{n}{112} - 3.5\right)\right)$$
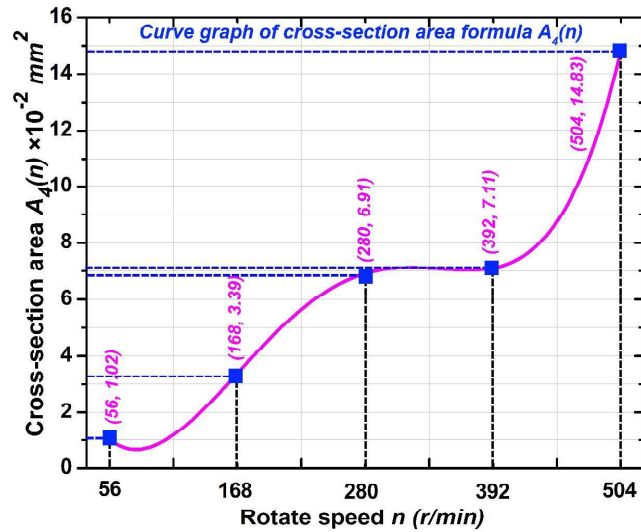
Fig.9 Curve graph of formula $A_4(n)$ of cross-section area of wear scar

at the different rotate speed n

Fig.10 showed the curve chart of prediction formula $W_4(n)$ of wear rate at the different rotate speed n. As was clear in **Fig.10**, wear rate exhibited the upward tendency with the increase of rotate speeds in the range of 56-280r/min, downward tendency in the region of 280-392r/min and ascending tendency in the district of 392-504r/min. In the range of 56-280r/min, the centrifugal force of wear debris was continually improved with the increasing of rotate speed n, leading to removing of wear debris from wear scar and increasing of wear rate of TiAl-10wt.%Ag. When the rotate speed n was improved from 280 to 504r/min, resulting in further improving of the centrifugal force of bulk wear debris, strengthening of the interaction forces between bulk wear debris and small wear debris, as well as random removing of small wear debris during the impacting process. Hence, the wear rate of TiAl-10wt.%Ag showed the fluctuant tendency with the increase of rotate speed n.
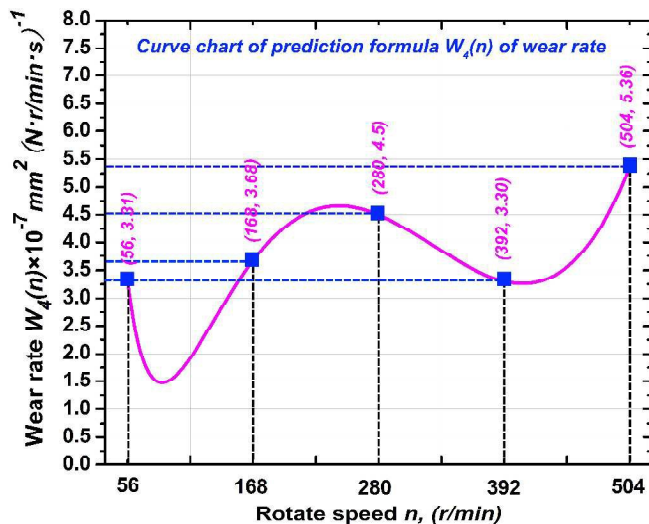
Fig.10 Curve chart of prediction formula $W_4(n)$ of wear rate

at the different rotate speed n

3.6.2 Evaluating prediction formula $W_4(n)$ of wear rate

Table 7 Comparative analysis between testing error and computational error at

9.15-**112**-3600 and 9.15-**448**-3600 (N-*r/min*-s)

Test conditions	9.15-**112**-3600			9.15-**448**-3600		
W_{test}	2.34	2.21	1.68	3.71	3.41	3.23
E_{test}	12.68%	6.42%	19.10%	7.54%	1.16%	6.38%
W_{comp}		2.07			3.59	
E_{comp}		0.32%			0.41%	

Table 7 showed the comparative analysis between testing error and computational

error at 9.15-**112**-3600 and 9.15-**448**-3600 (N-*r/min*-s). As shown in **Table 7**, the

testing error of wear rate showed the larger fluctuation at 9.15-**112**-3600, if compared

to 9.15-**448**-3600, leading to improving of testing error with the increasing of rotate

speed n. The smaller computational error was obtained than testing error at the

different rotate speed *n*. Hence, the prediction formula $W_4(n)$ of wear rate was accepted to predict wear rate in the district *[56r/min, 504r/min]*.

3.6.3 Influence of wear mechanisms on prediction accuracy
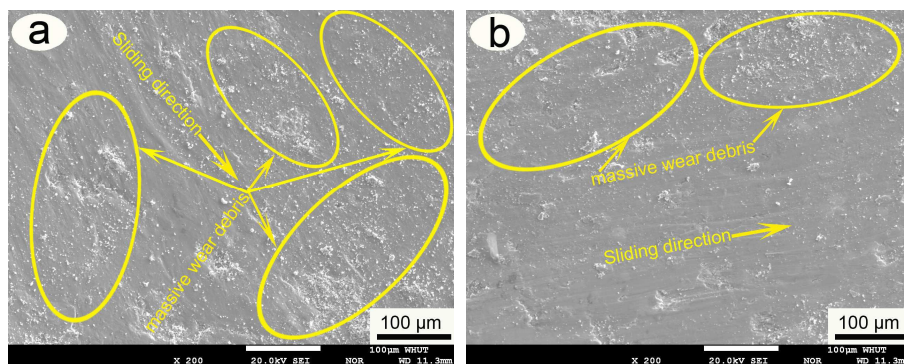
Fig.11 Representative electron probe morphologies of wear scar after 80min sliding at the different rotate speed *n*: 9.15-**112**-3600 (a), 9.15-**448**-3600 (b)

Fig.11 showed the representative electron probe morphologies of wear scar after 80min sliding at the different rotate speed *n*. Massive wear debris uniformly existed on smooth wear scar (see **Fig.11**a). It was evident that the primary wear mechanism was abrasive wear at 9.15-**112**-3600 (N-*r/min*-s). As shown in **Fig.11**b, a great deal of wear debris appeared on the the outward wear scar. It was evident that the primary wear mechanism was abrasive wear at 9.15-**448**-3600 (N-*r/min*-s). The centrifugal force of wear debris was continually improved with the increase of rotate speed *n*, resulting in improving of the centrifugal force of bulk wear debris, strengthening of the interaction forces between bulk wear debris and small wear debris, random removing of small wear debris during the impacting process, acquiring of the wear mechanism of abrasive wear, fluctuating of wear rate of TiAl-10wt.%Ag and lowering of prediction accuracy (from 99.68% to 99.59%) of formula $W_4(n)$ (see **formula 21**).

3.6.4 Influence of surface textures on prediction accuracy
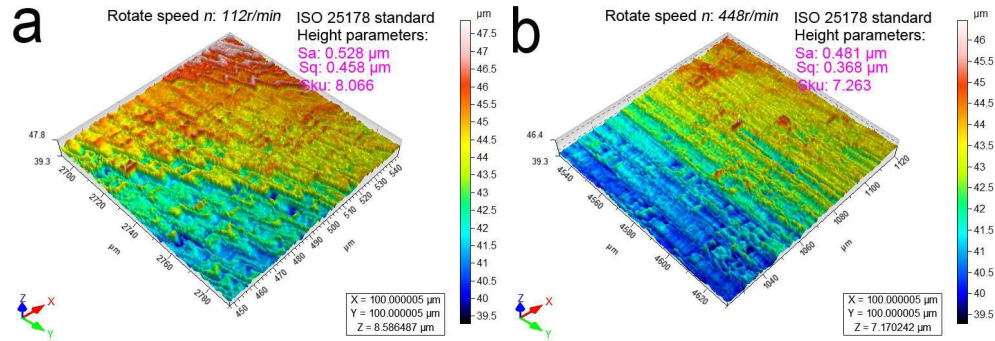
Fig.12 Typical surface texture of wear scar at the different rotate speed *n*:

9.15-**112**-3600 (a), 9.15-**448**-3600 (b)

Fig.12 showed the typical surface texture of wear scar at the different rotate speed

n. The smooth wear scar was obtained for the excellent height parameters of Sa (0.481

μm), Sq (0.368 μm) and Sku (7.263) at 9.15-**448**-3600 (N-*r/min*-s). The centrifugal

force of wear debris at 9.15-**448**-3600 was larger than at 9.15-**112**-3600, leading to

improving of remove of wear debris, strengthening of smoothness of wear scar,

fluctuating of wear rate of TiAl-10wt.%Ag and lowering of prediction accuracy (from

99.68% to 99.59%) of formula $W_4(n)$.

In order to evaluate the using longevity of mechanical component, It was necessary

to investigate wear rates at the different sliding time *t*.

3.7 Sliding time t

3.7.1 Constructing prediction formula $W_4(t)$ of wear rate

Before constructing prediction formula $W_4(t)$ of wear rate, cross-section area

formula $A_4(t)$ ($A_4(t)$ between *A* and *t*) was required to firstly construct by the method

of Newton interpolation.

Five interpolation points of *(900, 2.40 $\times 10^{-2}$), (1800, 4.90 $\times 10^{-2}$), (2700, 7.09 $\times$*

24

10^{-2}), (3600, 7.11×10^{-2}) and (4500, 6.24×10^{-2}) was chosen to construct cross-section

area formula $A_4(t)$ using the Newton interpolation method. **Table 5** showed the

forward differences at the different sliding time t. Hence, the forward differences was

employed to construct cross-section area formula $A_4(t)$, as shown in **formula 22**:

$$A_4(t) = A_4(t_0 + e_t \cdot h_t) = (2.40 + 2.5 \cdot \left(\frac{t}{900} - 1\right) - 0.155 \cdot \left(\frac{t}{900} - 1\right) \cdot$$
$$\left(\frac{t}{900} - 2\right) - 0.31 \cdot \left(\frac{t}{900} - 1\right) \cdot \left(\frac{t}{900} - 2\right) \cdot \left(\frac{t}{900} - 3\right) + 0.131 \cdot \qquad (22)$$
$$\left(\frac{t}{900} - 1\right) \cdot \left(\frac{t}{900} - 2\right) \cdot \left(\frac{t}{900} - 3\right) \cdot \left(\frac{t}{900} - 4\right)) \times 10^{-2}$$

Table 5 Forward differences at the different sliding time t

Sliding time t	$A(t)$	$\Delta A(t)$	$\Delta^2 A(t)$	$\Delta^3 A(t)$	$\Delta^4 A(t)$
900 (t_0)	2.40×10^{-2}	2.50×10^{-2}	-0.31×10^{-2}	-1.86×10^{-2}	3.14×10^{-2}
1800 (t_1)	4.90×10^{-2}	2.19×10^{-2}	-2.17×10^{-2}	1.28×10^{-2}	
2700 (t_2)	7.09×10^{-2}	0.02×10^{-2}	-0.89×10^{-2}		
3600 (t_3)	7.11×10^{-2}	-0.87×10^{-2}			
4500 (t_4)	6.24×10^{-2}				

Fig.13 showed the curve graph of formula $A_4(t)$ of cross-section area of wear scar at

the different sliding time t. Cross-section area A exhibited the upward tendency, when

sliding time t continuously increased in the range of 900-4500s.

In the sliding time district *[900s, 4500s]*, predicted formula $W_4(t)$ of wear rate was

written as **formula 23** by substituting cross-section area **formula** $A_4(t)$ (see **formula**

22) into **formula 7:**

$$W_s(t) = \frac{60}{F \cdot n \cdot t} \cdot A_4(t) = \frac{50}{2989 \cdot t} \cdot \times 10^{-2} \cdot \left(2.40 + 2.5 \cdot \left(\frac{t}{900} - 1\right) - 0.155 \cdot\right.$$

$$\left(\frac{t}{900} - 1\right) \cdot \left(\frac{t}{900} - 2\right) - 0.31 \cdot \left(\frac{t}{900} - 1\right) \cdot \left(\frac{t}{900} - 2\right) \cdot \left(\frac{t}{900} - 3\right) + 0.131 \cdot \tag{23}$$

$$\left.\left(\frac{t}{900} - 1\right) \cdot \left(\frac{t}{900} - 2\right) \cdot \left(\frac{t}{900} - 3\right) \cdot \left(\frac{t}{900} - 4\right)\right)$$
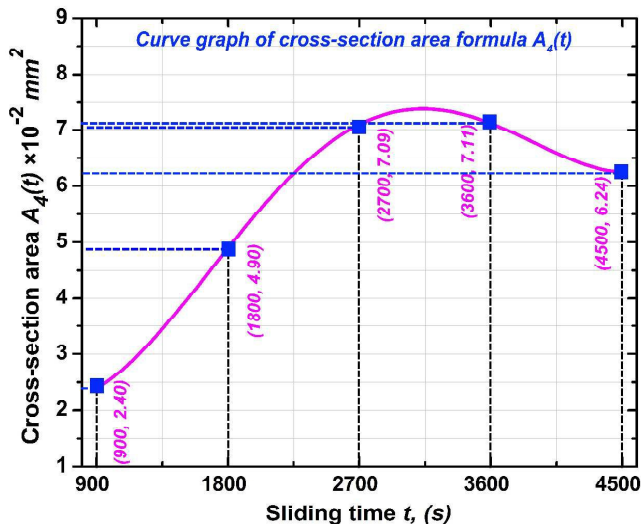
Fig.13 Curve graph of formula $A_4(t)$ of cross-section area of wear scar
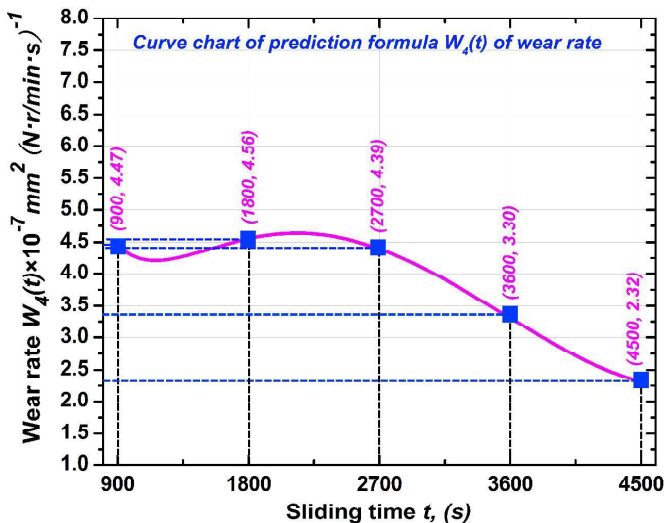
at the different sliding time t

Fig.14 Curve chart of prediction formula $W_4(t)$ of wear rate

at the different sliding time t

Fig.14 exhibited the curve chart of prediction formula $W_4(t)$ of wear rate at the different sliding time t. As shown in **Fig.14**, wear rate constantly decreased with the increase of sliding time t. Bulk wear debris was repeatedly crushed into a great deal of small wear debris with the increase of sliding time t, resulting in incessant forming of anti-friction film and continuous lowering of wear rate of TiAl-10wt.%Ag.

3.7.2 Evaluating prediction formula $W_4(t)$ of wear rate

Table 8 Comparative analysis between testing error and computational error at

9.15-392-**1350** and 9.15-392-**4050** (N-r/min-*s*)

Test conditions	9.15-392-**1350**			9.15-392-**4050**		
W_{test}	4.51	4.11	3.89	2.80	2.67	2.50
E_{test}	8.15%	1.44%	6.71%	5.40%	0.50%	5.90%
W_{comp}		4.27			2.72	
E_{comp}		2.40%			2.38%	

Table 8 showed the comparative analysis between testing error and computational error at 9.15-392-**1350** and 9.15-392-**4050** (N-r/min-*s*). As shown in **Table 8**, when the sliding time t increased from 1350 to 4050s, the testing error of wear rate was lowered at 9.15-392-**4050** than 9.15-392-**1350**. The computational error was smaller than testing error at the different sliding time t. Hence, the prediction formula $W_4(t)$ of wear rate was acceptant to predict wear rate in the sliding time district *[900s, 4500s]*.

3.7.3 Influence of wear mechanisms on prediction accuracy

Fig.15 showed the representative electron probe morphologies of wear scar after 80min sliding at the different sliding time t. As was clear in **Fig.15**a, massive shallow

peeling pits and abrasive debris existed on wear scar. It was apparent that the primary

wear mechanisms were peeling and abrasive wear at 9.15-392-**1350** (N-r/min-*s*). As

shown in **Fig.15**b, shallow peeling pits and discontinuous wear grooves appeared on

the smooth wear scar at 9.15-392-**4050** (N-r/min-*s*). It was obvious that the primary

wear mechanisms were peeling and plough. Bulk wear debris was repeatedly crushed

into massive small wear debris with the increase of sliding time *t*, resulting in

incessant forming of anti-friction film, slight converting of wear mechanisms,

continuous lowering of wear rate of TiAl-10wt.%Ag, and stabilizing of prediction

accuracy (from 97.60% to 97.62%) of prediction formula $W_4(t)$ of wear rate (see

formula 25).
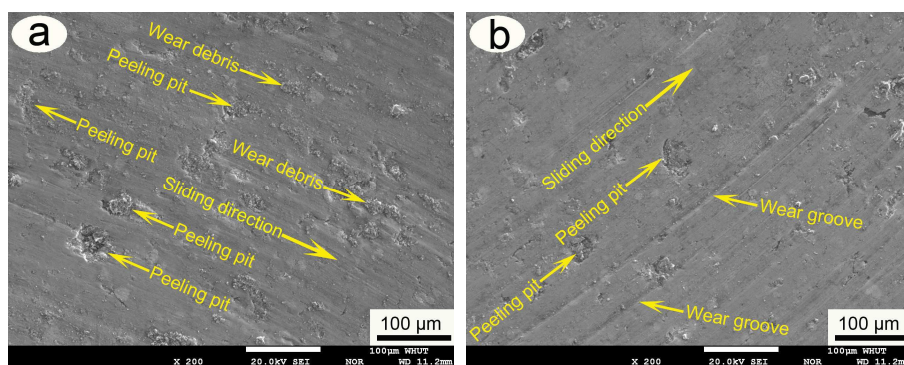
Fig.15 Representative electron probe morphologies of wear scar after 80min sliding at

the different sliding time *t*: 9.15-392-**1350** (a), 9.15-392-**4050** (b)

3.7.4 Influence of surface textures on prediction accuracy

  Fig.16 exhibited the typical surface texture of wear scar at the different sliding time *t*.

When sliding time *t* increased from 1350 to 4050s, the smooth wear scar was obtained

for the smaller height parameters of Sa (0.356 μm), Sq (0.291 μm) and Sku (6.241).

The small wear debris constantly formed for the reiterative crush with the increasing

of sliding time t, resulting in forming of anti-friction film, lowering of wear rate of

TiAl-10wt.%Ag and stabilizing of prediction accuracy (from 97.60% to 97.62%) of

prediction formula $W_4(t)$.
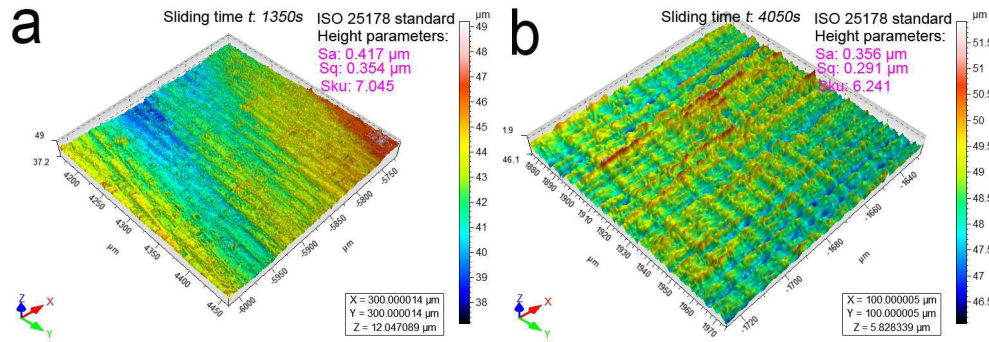
Fig.16 Typical surface texture of wear scar at the different sliding time t:

9.15-392-**1350** (a), 9.15-392-**4050** (b)

In this study, in order to study the variation of wear rate at the different applied

load F, rotate speed n and sliding time t, prediction formulas $W_4(F)$, $W_4(n)$ and $W_4(t)$

of wear rate were constructed based on TiAl-10wt.%Ag. Five interpolation nodes

were firstly chosen to respectively construct formulas $A_4(F)$, $A_4(n)$ and $A_4(t)$ ($A_4(F)$

between A and F, $A_4(n)$ between A and n, as well as $A_4(t)$ between A and t) using the

method of Newton interpolation. And then prediction formulas $W_4(F)$, $W_4(n)$ and $W_4(t)$

were obtained by substituting formulas $A_4(F)$ (see **formula 18**), $A_4(n)$ (see **formula 20**)

and $A_4(t)$ (see **formula 22**) into wear rate formula W_4 (see **formula 7**). Prediction

formulas $W_4(F)$, $W_4(n)$ and $W_4(t)$ of wear rate, which were evaluated by making a

comparison between computational error and testing error, could be accepted to

predict wear rate for the smaller computational error. Prediction accuracies of

formulas $W_4(F)$, $W_4(n)$ and $W_4(t)$ were respectively given the reasonable explanations

by wear mechanisms and surface texture at the different applied load F, rotate speed n

and sliding time t. It was found that the prediction accuracy of prediction formula of wear rate gradually increased for the higher binding force of wear debris at the larger applied load F (see formula $W_4(F)$), and slightly decreased for the random impacting between bulk wear debris and small wear debris at the higher rotate speed n (see formula $W_4(n)$), as well as relatively stabilized for the incessant forming of anti-friction film at the different sliding time t (see formula $W_4(t)$).

4. Conclusions

In the pure Ar atmosphere protection, TiAl-10wt.%Ag was fabricated by SPS for 8min at the temperature and pressure of 1000℃ and 30MPa. The formulas $W_4(F)$, $W_4(n)$ and $W_4(t)$, which were constructed by the Newton interpolation method, were respectively employed to predict wear rate with the increase of applied load F, rotate speed n or sliding time t at room temperature. The conclusions were obtained as follows:

1) Formulas $W_4(F)$, $W_4(n)$ and $W_4(t)$, which were constructed by the method of Newton interpolation, could be employed to predict wear rate for the smaller computational errors.

2) In the applied load district *[1.65N, 11.65N]*, the prediction accuracy of formula $W_4(F)$ gradually increased for the higher binding force of wear debris at the larger applied load F.

3) The prediction accuracy of formula $W_4(n)$ slightly decreased for the random impacting between bulk wear debris and small wear debris at higher rotate speed n.

4) In the sliding time district *[900s, 4500s]*, the prediction accuracy of formula $W_4(t)$

relatively stabilized for the incessant forming of anti-friction films.

5) The prediction formulas $W_4(F)$, $W_4(n)$ and $W_4(t)$ in the form of Newton interpolation polynomial can be respectively adopted to predict wear rate with the increase of applied load F, rotate speed n and sliding time t, in order to evaluate the using longevity of mechanical components in the industrial fields.

Acknowledgments

References

1 S.Y. Sung, Y.J. Kim, Intermetallics, 2007, **15,** 468.

2 X.H. Wu, Intermetallics, 2006, **14**, 1114.

3 C.M. Austin, Curr. Opin. Solid State Mater. Sci, 1999, **4**, 239-242.

4 F.H. Fores, C. Suryanarayana, D. Eliezer, J Mater Sci, 1992, **27**, 5113.

5 T. Sun, Q.D. Wang, L. Sun, G.H. Wu, Y. Na, Wear, 2010, **268**, 693.

6 X.L. Shi, Z.S. Xu, M. Wang, W.Z. Zhai, J. Yao, S.Y. Song, Wear, 2013, **303(1-2)**, 486.

7 J.F. Archard, J. Appl. Phys, 1953, **24**, 981.

8 P. Kishore Sampathkumaran, S. Seetharamu, S. Vynatheya, A. Murali, Wear, 2000 **237**, 20.

9 Y. Y. Boneh, A. Sagy, Z. Reches, Earth Planet Sc Lett, 2013, **381**,127.

10 S. Kasolang, M. A. Ahmad, F. A. Ghazali, A. M. Azmi, Appl Mech Mater, 2011 52, 464.

11 K. Gong, H.L. Luo, D. Feng, C.H. Li, Wear, 2008, **265**, 1751.

12 Q. Cui, J. Shu, Z.F, Wu, G.X. Jiang, Power Electronics, 2013, **47(7)**, 46.

13 ASTM E92-82, Standard test method for vickers hardness of metallic materials, ASTM International, 2003.

14 ASTM B962-08, Standard test methods for density of compacted or sintered powder metallurgy (PM) products using Archimedes' principle, ASTM International, 2008.

15 ASTM G99-95, Standard test method for wear testing with a pin-on-disk apparatus, ASTM International, 1995.

16 C.X. Li, J. Xia, H. Dong, Wear, 2006, **261**, 693.

17 M.Y. Huang, B. Liu, T. Xu, Science publishing company, 2005.